MATERIALS CHEMISTRY
FRONTIERS

CCS 中国化学会 CHINESE CHEMICAL SOCIETY
ICCAS
ROYAL SOCIETY OF CHEMISTRY

RESEARCH ARTICLE

View Article Online
View Journal | View Issue

Cite this: *Mater. Chem. Front.*, 2024, **8**, 1950

Intrinsically stretchable and efficient cross-linked small molecular emitter for flexible organic light-emitting diodes†

Ning Sun,‡[a] Xiang An,‡[b] Jianye Gong,[a] Yingying Zheng,[b] Lubing Bai,[b] Huaqiang Gong,[b] Yahui Zhang,[b] Mingjian Ni,[b] Zhiqiang Zhuo,[b] Chuanxin Wei,[c] Man Xu,[c] Jianguo Wang,*[a] Yamin Han,*[b] Wei Huang[abc] and Jinyi Lin *[b]

Due to their rigid and plane conjugated skeletons, small molecular semiconductors always present irreversible brittle properties in the nano-film state, which is not conducive to deformation and operation stability in flexible optoelectronic devices. Herein, we proposed a universal side-chain cross-linkable strategy to construct a dynamic network structure of a small molecular semiconductor (F-3OCm) to improve the deformation tolerance for the fabrication of flexible optoelectronic devices. First, model F-3OCm cross-linked films were obtained by thermal annealing, which presented perfect solvent resistance. Compared to control F-3OEt, F-3OCm cross-linked films displayed viscoelastic behavior with low Young's modulus. Additionally, the tensile fracture rates of F-3OCm cross-linked films are enhanced to ~20% without obvious cracks, indicating the excellent intrinsic stretchability with excellent deformation stability. In addition, these stretchable films present not only efficient emission behavior with a PLQY of ~50% but also have deep-blue emission with tension-ratio-independent color purity. Finally, flexible organic light-emitting diodes (OLEDs) based on the F-3OCm cross-linked films present excellent deformation stability, associated with their intrinsically stretchabilty. Therefore, the side-chain cross-linkage strategy is a promising approach for designing intrinsically stretchable small molecular semiconductor films for flexible electronics.

Received 30th December 2023,
Accepted 9th February 2024

DOI: 10.1039/d3qm01349a

rsc.li/frontiers-materials

Introduction

Emerging flexible organic electronic devices are widely applied in the field of optoelectronic equipment, such as displays, wearable and bio-electronic devices, due to their advantages of ultrathin dimensions, knittability, stretchability and applicability.[1–15] However, due to the brittleness of traditional rigid conjugated materials, imbalanced stress on the upper and lower surfaces of functional nano-layers easily occurs under device deformation such as bending, stretching or folding.[16–19] These intralayer internal forces and unmatched mechanical properties may cause film fracture and slippage, leading to device failure, which is an important bottleneck limiting the practical application of traditional organic semiconductors in flexible optoelectronics.[20,21] Therefore, enhancing the ability of functional layers to resist device deformation is an effective strategy to improve the long-term deformation and operation stability of flexible optoelectronic devices.[16,19,22–24] At present, common strategies include using a flexible ultra-thin substrate to construct a pleated luminescent layer, which pre-stretches the flexible substrate during the process of device preparation.[23–27] However, the flexibility and stretchability obtained by external interference are random, with a lack of stability and controllability and are not suitable for the fabrication of large-area and arrayed flexible optoelectronic devices. Therefore, it is necessary to achieve intrinsic flexibility in organic semiconductor layers to enhance the strain stability and optoelectrical properties of flexible optoelectronic devices.

In general, establishing an energy dissipation centre is crucial for enhancing the capacity of organic conjugated molecules to resist device deformation in flexible electronics.[7,16,22,28–32] It is well known that the interpenetration and entanglement of conjugated polymeric chains presents the potential for intrinsic stretchability in the solid state.[3,12,22,28,31,33–38] As an alternative to

[a] *Country College of Chemistry and Chemical Engineering, Inner Mongolia Key Laboratory of Fine Organic Synthesis, Inner Mongolia University, Hohhot 010021, China. E-mail: wangjg@iccas.as.cn*
[b] *State Key Laboratory of Organic Electronics and Information Displays, Nanjing University of Posts and Telecommunications, Nanjing 210023, China. E-mail: iamymhan@njtech.edu.cn, iamjylin@njtech.edu.cn*
[c] *Key Laboratory of Flexible Electronics (KLOFE) & Institute of Advanced Materials (IAM), Nanjing Tech University (NanjingTech), Nanjing 211816, China*

† Electronic supplementary information (ESI) available. See DOI: https://doi.org/10.1039/d3qm01349a

‡ Ning Sun and Xiang An contributed equally to this work.

π-conjugated polymers, small-molecule semiconductors are easily synthesized and functionalized with a definite chemical structure, which endows the materials with unique physical, chemical and photoelectric properties.[28,39–43] However, small molecules mainly tend to self-assemble and densely pack together, which may cause brittle fracture behaviour in their deposited thin films.[39,40,44,45] Additionally, although the introduction of a flexible side chain may allow for the proper viscosity to obtain excellent solution -process ability for the fabrication of optoelectronic devices, the relatively loose and isolated intermolecular arrangement also causes the easy tensile failure of nano-films.[18,46–48] It is extremely impossible to fabricate a flexible electronic device with excellent deformation stability based on small-molecule semiconductors.[16,47,49] Herein, we propose a universal side-chain cross-linking strategy to obtain intrinsically stretchable small-molecule films with anti-deformation ability for solution-processed flexible organic light-emitting diodes (OLEDs). First, a model small-molecule emitter, F-3OCm with three cross-linkable styrene units is designed and prepared, together with F-3OEt as a control, as shown in Fig. 1. More interestingly, compared to extremely brittle F-3OEt and F-3OCm pristine films, the F-3OCm cross-linked film showed excellent intrinsically stretchability with a tensile rate of ~20% and efficient emission behaviour with a PLQY of ~50%. Additionally, stretchable F-3OCm films also show a low Young's modulus with excellent recoverability, according to the nanoindentation measurement. Finally, this cross-linked emissive layer also presents excellent device deformation stability in flexible OLEDs.

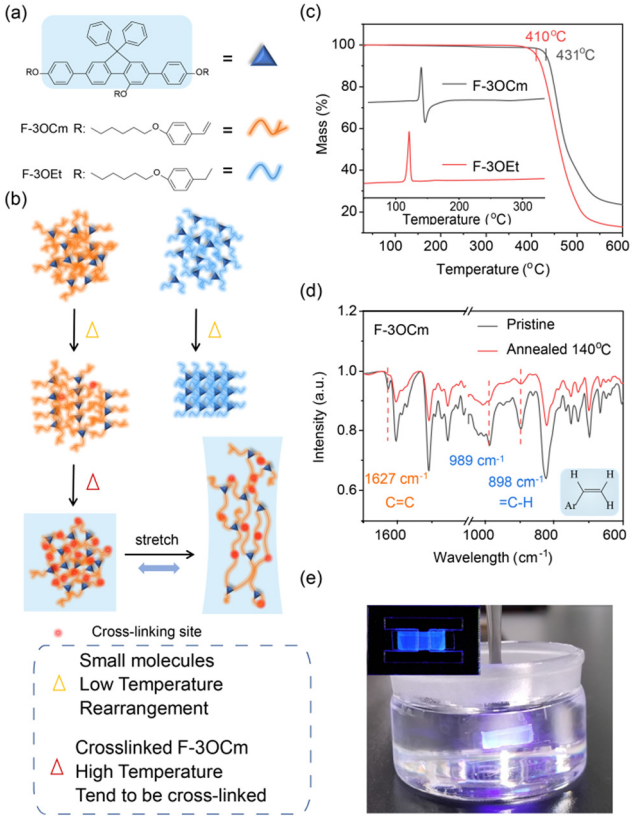

Fig. 1 Universal side-chain cross-linking strategy to obtain intrinsically stretchable small-molecule conjugated materials. (a) Chemical structures of F-3OCm and F-3OEt. (b) Possible behavior of different small-molecule materials after thermal annealing treatment, and a diagram of crosslinked small molecules after crosslinking. (c) TGA curves of F-3OCm and F-3OEt. Inset shows the partial DSC curves of F-3OCm and F-3OEt. (d) FT-IR curves of pristine F-3OCm powder and the film annealed at 140 °C. (e) Experiments on solvent resistance in toluene: substrate-free F-3OCm film annealed at 140 °C (annealing time: 10 min).

Results and discussion

Similar to dynamic physical crosslinks in polymers, building a chemical network in small-conjugated-molecule films is an effective method to enhance their stress-deformation stability for flexible electronic devices.[28,30,32,48] Therefore, thermally cross-linkable styryl units are introduced into steric fluorene segments to construct a network in solid films, which may substantially improve their stretchability. Therefore, two small-molecule emitters, F-3OCm and F-3OEt, were designed and prepared, as shown in Fig. 1a. The specific reaction routes and synthesis steps are provided in the ESI.† The chemical structures of intermediates and target products were confirmed using nuclear magnetic resonance spectroscopy (NMR) and mass spectrometry (Fig. S1–S8, ESI†). From thermogravimetric (TGA) curves, the decomposition temperatures (T_d) of F-3OCm and F-3OEt were estimated to be about 431 °C and 410 °C, respectively (Fig. 1c). Differential scanning calorimetry (DSC) measurements showed that F-3OEt had a sharp endothermic peak between 108 °C and 126 °C. From the curve profile of exothermic behavior, it can be determined that solidification, oxidation, reaction or crosslinking may occur under thermal treatment during DSC measurements. The introduction of crosslinked styryl units enables F-3OCm to form a cross-linked network under thermal treatment. According to DSC results, temperatures of 120 °C and 140 °C were selected to induce the cross-linking processing of F-3OCm in the film states. As expected, the data in Fig. 1d clearly showed that the ═C–H out-of-plane oscillating vibration absorption peaks of F-3OCm appeared at 898 cm^{-1} and 989 cm^{-1}, together with the C═C stretching vibration absorption peak at 1627 cm^{-1}.[48,50] In comparison, it can be found that after annealing at 140 °C for 10 min, the absorption intensity of the RCH = CH_2 feature of F-3OCm annealed films decreased significantly, effectively supporting the intermolecular cross-linked reaction (Fig. S9, ESI†). Therefore, it was effectively concluded that intermolecular chemical networks were achieved in the annealed F-3OCm films under thermal treatment.

In general, intrinsically flexible nano-films always show excellent deformation stability under stress. Subsequently, we also tried to obtain substrate-free films of the two emitters *via* the stripping method.[51] It should be noted that the key step was dissolving the substrate PEDOT:PSS layer in water and further separating emission films in the water.[51] In this procedure, brittle independent nano-films are easily broken on the surface of water due to the internal surface stress. As expected, the F-

3OCm and F-3OEt pristine films cannot be easily obtained *via* this method due to their intrinsic brittleness. More interestingly, the annealed F-3OCm films obtained *via* thermal treatment at 140 °C and 180 °C were achieved *via* this conventional stripping method. Additionally, the pristine films of F-3OEt and F-3OCm were directly dissolved in common organic solvents, such as toluene and dichloromethane (Fig. S10 and Movies S1, S2, ESI†). As expected, the F-3OCm annealed films completely maintained the film morphology after being immersed in toluene (Fig. 1e). The difference between them was that the annealed F-3OCm film obtained at 140 °C showed a slightly more obvious degree of shrinkage in toluene solvent than the film obtained at 180 °C. Additionally, dissolved F-3OCm molecules in toluene present blue emission under irradiation with a 360-nm ultraviolet lamp (Fig. S10 and Movies S3, S4, ESI†). F-3OCm films with different degrees of crosslinking can be obtained by controlling the thermal annealing temperature. Therefore, the substrate-free annealed F-3OCm films with excellent solvent resistance also supported the formation of a crosslinked network, which is a key factor to obtain stretchability.

Film morphology is a key parameter to improve the optoelectronic properties and stretching behavior of spin-coated active nano-films.[34] Therefore, optical microscopy and atomic force microscopy (AFM) measurements were explored to further reveal the surface morphology of the pristine and annealed F-3OCm films, together with the that of the pristine F-3OEt film. First, the optical microscopy images clearly showed that all four films displayed a smooth surface morphology. All films also exhibited uniform and efficient deep-blue emission under ultraviolet lamp irradiation, further confirming the excellent smooth morphology (Fig. 2a and Fig. S11, ESI†). More interestingly, as shown in AFM images in Fig. 2a, the pristine F-3OCm and F-3OEt films have a smooth film morphology with an extremely small roughness (R_q: 0.298 nm, R_a: 0.231 nm for F-3OCm, R_q: 0.274 nm, R_a: 0.218 nm for F-3OEt). The surface morphology of F-3OCm was slightly rougher after thermal annealing at 140 °C and 180 °C (R_q: 1.724 nm, R_a: 1.374 nm for the F-3OCm film annealed at 140 °C, R_q: 2.251 nm, R_a: 1.790 nm for the F-3OCm film annealed at 180 °C). In addition, to further verify the solvent resistance of the annealed cross-linked F-3OCm film, toluene was dropped onto the annealed film to explore the effect of secondary spin-coating processing on the film morphology. The experimental results perfectly verified the solvent resistance of crosslinked F-3OCm films annealed at 140 °C and 180 °C. Compared to the annealed film obtained at 180 °C, the film thickness was slightly decreased after the secondary spin-coating processing for the film obtained using thermal treatment at 180 °C (Fig. S12, ESI†). More interestingly, the surface morphology of the crosslinked film was improved to some extent after a second coating processing with toluene. In summary, the crosslinked F-3OCm film presents an excellent and uniform surface morphology without obvious defect structures, which is essential for the enhancement of its stretchability and emission behavior for the fabrication of flexible optoelectronic devices.

Then, to describe the stretchability properties of the crosslinked F-3OCm films, the spin-coated films were transferred to a PDMS substrate, and their tensile properties were visually measured using a biaxial tensile test. The surface cracks in the films were observed under optical microscopic measurements. In the initial state, the surface of the film is smooth without obvious cracks (Fig. 2a and Fig. S13, ESI†). When the films were slowly stretched to 4%, the pristine F-3OCm and F-3OEt films, which were even annealed at 60 °C (to remove the residual solvent), began to show a large number of obvious cracks. As expected, the tensile properties of the F-3OCm films obtained by thermal annealing at 140 °C and 180 °C were greatly improved. The crack point of the film cross-linked at 140 °C appeared only when it was slowly stretched to 12%, and the cracks grew slowly as the stretching continued. The stretchability properties of the crosslinked F-3OCm films obtained after thermal annealing at 180 °C are better, with cracks only appearing when the strain is 16%. Therefore, the side-chain crosslinking behaviour of small-molecule emitters can greatly improve their stretchability properties in the thin-film state. In addition, SEM images clearly showed that the fracture surface of the pristine F-3OCm film after stretch processing is flat and smooth, suggesting obvious brittle fracture properties (Fig. 2b).[22,36] The tensile fracture surface of the cross-linked film obtained by thermal annealing at 180 °C was rough and

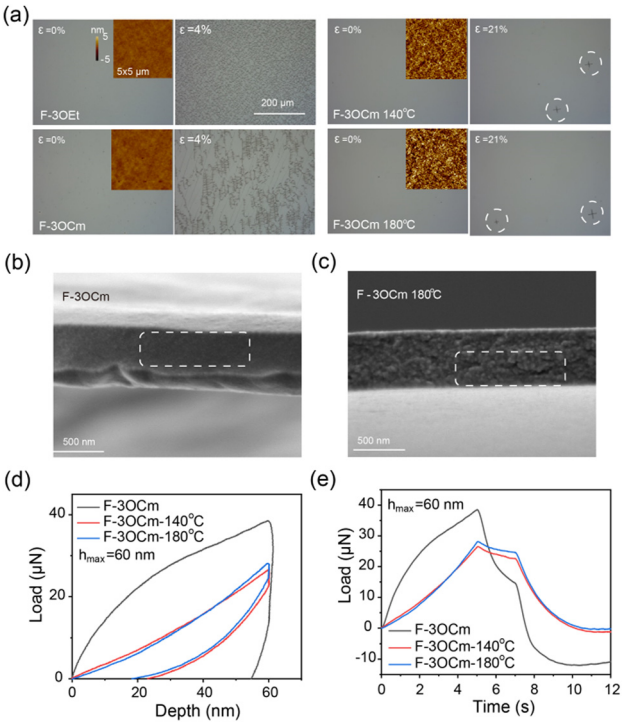

Fig. 2 Morphology characterization and qualitative mechanical properties of F-3OCm and F-3OEt films. (a) Optical microscopy images of the F-3OCm films obtained after annealing at 60 °C, 140 °C and 180 °C, as well as the F-3OEt film annealed at 60 °C upon the application of stress with a stretch rate of 0%, 4% and 21%. The insets illustrate corresponding AFM images. Cross-section SEM images of the pristine (b) and annealed (c) F-3OCm films after tensile fracture. (d) Load-depth curves (h_{max} = 60 nm) and (e) load-time curves (60 nm) of the pristine F-3OCm film and the F-3OCm films obtained by annealing at 140 °C and 180 °C in constant displacement rate mode.

cracked, showing ductile fracture (Fig. 2c). In our assumption, F-3OCm and F-3OEt molecules are in the individual state in the pristine films, which may result in the brittle fracture under tensile processing. Interestingly, the intermolecular network that appeared in the cross-linked F-3OCm film can dissipate this external stress energy to resist physical deformation, which may improve its stretchability. Therefore, the introduction of side-chain cross-linked groups into small-molecule compounds is helpful to substantially improve their stretchability properties in the film state.

Finally, the quantitative mechanical properties of the F-3OEt and F-3OCm films were explored *via* nano-indentation in two operation modes, namely, constant displacement rate mode and constant loading rate mode.[22,38] As shown in Fig. 2d, e and Fig. S14, S15 (ESI†), the maximum load (P_{max}) of the pristine F-3OCm film and the F-3OCm films annealed at 140 °C and 180 °C are 33, 31 and 32 μN, respectively. From the two modes of nanoindentation testing, it can be clearly found that the pristine F-3OEt and F-3OCm films displayed different mechanical behaviours, while both the crosslinked annealed films show similar mechanical behaviours. The pristine F-3OCm film showed different unloading behaviour under constant loading rate mode. In the process of gradually removing external force, residual strain still occurs, showing typical deformation behaviour (Fig. S16, ESI†). Additionally, the cross-linked F-3OCm films have similar hardness, but the cross-linked film obtained through treatment at 180 °C has a higher Young's modulus. The Young's modulus under constant displacement rate mode is 3.00 GPa for the F-3OCm film annealed at 140 °C but increases to 3.46 GPa for the F-3OCm film annealed at 180 °C. F-3OEt has the highest Young's modulus (48.65 Gpa) and hardness (6.95 Gpa), indicating its brittleness and rigidity(Table S1, ESI†). It is noteworthy that the F-3OCm films annealed at 140 °C and 180 °C showed mechanical relaxation during the retention process, reflecting their slightly viscoelastic properties (Fig. 2d and e). Furthermore, the three-parameter model was used here to fit the stress relaxation and creep behaviour under the two modes, respectively. The model provided further parameters P_0 and P_1 (5.38 and 21.30 μN for the F-3OCm film annealed at 140 °C and 4.30 and 24.19 μN for the F-3Ocm film annealed at 180 °C), which can characterize their viscoelasticity and elasticity, as well as the displacement D_0 caused by viscoelasticity under pressure and the displacement D_1 caused by elastic deformation and structural damage under pressure (Table S2 and Fig. S17, ESI†). The elasticity contributes to the real displacement, D_1'. D_1' is obtained from D_1 minus the unrecoverable form variable of the constant loading rate mode. According to obtained parameter data, ratios P_1:P_0 (5.63) and D_1':D_0 (7.85) for the F-3OCm film annealed at 180 °C are both larger than those of the film annealed at 140 °C (3.96 for P_1:P_0 and 6.76 for D_1':D_0), indicating that the crosslinked film annealed at higher temperature has greater elasticity and viscoelasticity, consistent with previous conclusions. All above observations effectively support the intrinsic viscoelasticity of the F-3OCm cross-linked films, which also enables them to have excellent stretching behaviour.

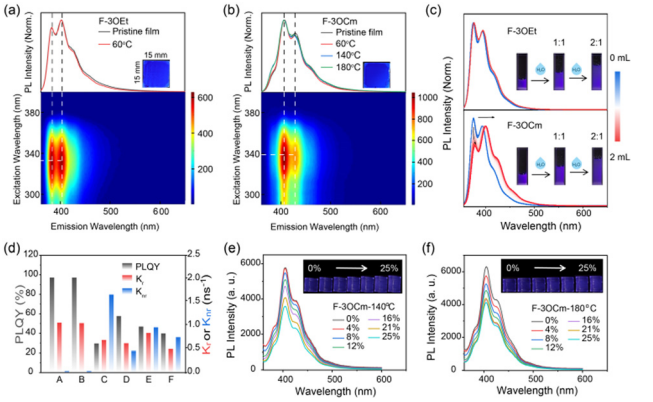

Fig. 3 Optical properties of F-3OCm and F-3OEt in various states. (a) and (b) PL spectra of films of F-3OEt and F-3OCm in the pristine state and after annealing at 60 °C, 140 °C or 180 °C. The bottom parts are the 3D PL mapping of the pristine F-3OEt and F-3OCm films. (c) PL spectra of F-3OEt and F-3OCm in THF solution. After each test, 50 μL of H_2O was successively added to the solution, which was then tested after mixing evenly. The insets are images of the initial solution in the colorimetric dish under an ultraviolet lamp with the addition of 0 mL, 1 mL and 2 mL H_2O, respectively. (d) PLQY, radiation transition rate (k_r) and non-radiative transition rate (k_{nr}) of toluene solutions of F-3OEt (A) and F-3OCm (B), the pristine F-3OEt film (C), the pristine F-3OCm film (D), and the F-3OCm films annealed at 140 °C (E) and 180 °C (F). (e) and (f) Tensile spectra and photos of F-3OCm films annealed at 140 °C and 180 °C on PDMS substrates. The tensile rates were 0%, 4%, 8%, 12%, 16%, 21% and 25%, respectively.

Next, the optical properties of F-3OEt and F-3OCm in solution and thin films were systematically explored to investigate their photophysical properties. As shown in Fig. 3, the UV-vis absorption and emission spectra of diluted F-3OCm and F-3OEt solutions are basically identical due to their similar conjugated backbone structures. The maximum absorption peak is estimated to be located at about 337 nm. Additionally, the PL spectra of the two diluted solutions consisted of three emission peaks at 375 nm, 393 nm and 412 nm, respectively, indicating single-molecule emission behavior (Fig. S18, ESI†). Surprisingly, the absorption and emission spectra of the pristine F-3OCm and F-3OEt films differ considerably from the solution-state ones. As shown in Fig. S11 (ESI†), the pristine F-3OCm and F-3OEt films showed efficient and uniform ultra-deep-blue emission. The maximum absorption peak of the F-3OCm and F-3OEt film was located at about 343 nm. However, the main fluorescence emission peaks of F-3OCm are 405 nm and 427 nm, together with two shoulder emission peaks at 385 nm and 451 nm. The PL spectra of the spin-coated F-3OEt films consisted of two emission peaks at 381 nm and 401 nm and shoulder peaks at 417 nm and 445 nm. Besides, 3D PL mapping analysis confirmed this assumption. It is noteworthy that the annealed F-3OCm and F-3OEt films also exhibited the same photophysical behavior as the pristine films (Fig. 3a, b and Fig. S19, ESI†), indicating their excellent spectral stability toward temperature. All the pristine and annealed F-3OCm and F-3OEt films displayed deep-blue emission. More interestingly, there is weak intermolecular aggregation in the F-3OCm film, which may reasonably explain the slightly stronger emission intensity at the

0–1 emission band compared to the 0–0 band. To verify the above conjecture, the intermolecular aggregation-dependent emission of F-3OCm and F-3OEt were explored *via* the addition of the poor solvent water (H_2O) in THF solution (Fig. 3c). The emission behavior of the dilute THF solution of F-3OCm is similar to that of F-3OEt. Compared to the similar emission spectrum profile of F-3OEt, the intensity ratio of the 0–1/0–0 band emission increases after adding H_2O, also confirming the intermolecular aggregation in the film state. In addition, as presented in Fig. S20 (ESI†), the fluorescence lifetimes of the dilute solutions of F-3OCm and F-3OEt at 420 nm were estimated to be about 900 ps, but decreased to 600–800 ps for the pristine films. The fluorescence lifetime corresponding to the three emission peaks of the pristine F-3OEt film was completely different, which indicates that F-3OEt has more than one luminous center in the film state. The fluorescence lifetimes of the pristine and annealed films of F-3OCm were similar; the annealed F-3OCm film also had a similar lifetime with a value of 600–800 ps. In addition, the dilute solutions of F-3OCm and F-3OEt had relatively high PLQY of 97.2% and 97.1%, respectively. However, this value was seriously reduced to about 30% for the pristine F-3OEt films (Fig. 3d and Table S3, ESI†). More interestingly, the pristine and annealed F-3OCm films also showed robust deep-blue emission with PLQY values of 57.6% and 46.9%. In addition, we further investigated the effect of stretching rate on the luminescence behavior of the crosslinked F-3OCm films. The fluorescence emission intensity of the F-3OCm films annealed at 140 °C and 180 °C gradually decreased with increasing tensile ratio, while the emission peak wavelength was basically unchanged, also suggesting excellent deep-blue emission (Fig. 3e and f). Therefore, the stretchable cross-linked F-3OCm film presents efficient and stable deep-blue emission.

As discussed above, the crosslinked F-3OCm film simultaneously presents robust emission behaviour and stretchability, which are crucial for the construction of flexible OLEDs with excellent deformation stability. Therefore, we further fabricated flexible OLEDs to check this assumption. First, the highest occupied orbital (HOMO) and the lowest vacant orbital (LUMO) of F-3OCm and F-3OEt were determined to be −5.33 eV and −2.37 eV and −5.33 eV and −2.34 eV, respectively, from CV curves (Fig. S22, ESI†). Preliminary flexible OLEDs were prepared on a flexible PI substrate with the configuration ITO/PEDOT:PSS/EML (F-3OCm or F-3OEt)/TPBi/LiF/Al. As expected, F-3OEt-based flexible OLEDs were prone to failure during the bending process, which is related to the brittle and crack properties of luminescent layer (Movie S5, ESI†), while corresponding F-3OCm-based flexible OLEDs had good bendability. The uncontrollable interlayer forces in the flexible OLEDs based on the F-3OCm cross-linked films under device deformation have a slight influence on the device performance. Therefore, this type of flexible OLEDs has better bendability and luminous uniformity (illustration in Fig. 4c and Movies S6–S8, ESI†). Furthermore, we separated the luminescence layer and hole transport layer of the flexible OLEDs to explore the film morphology of the luminescence layer after repeated bending. In the initial state, the emission layers of F-3OCm and F-3OEt

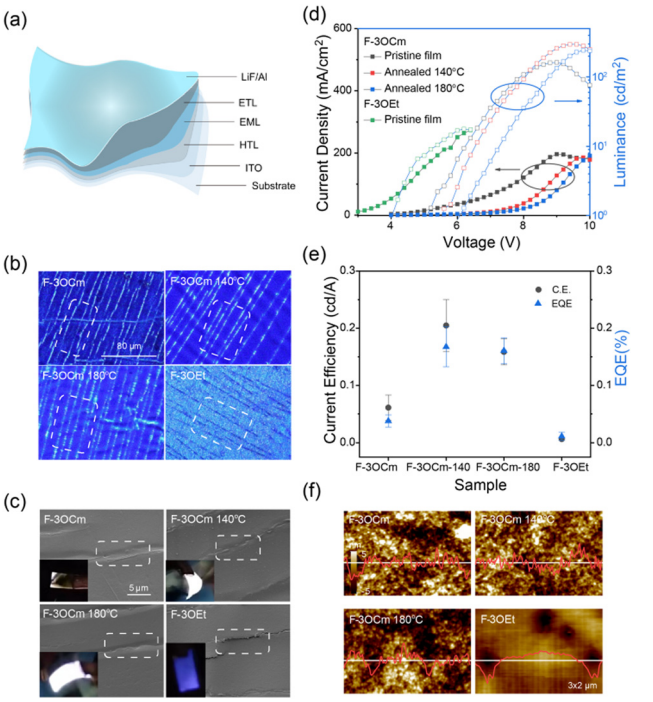

Fig. 4 (a) Configuration structure of small-molecule-based flexible OLEDs. Fluorescence microscopy (b) and SEM (c) images of the interior of the OLED devices before fatigue. (d) Current density–luminance–voltage characteristics of the flexible devices. (e) Current efficiency and external quantum efficiency error diagrams of flexible devices based on the pristine F-3OCm film, the F-3OCm films annealed at 140 °C and 180 °C, and the pristine F-3OEt film. (f) Atomic force microscopy (AFM) characterization of the emitting layers of the flexible devices based on the pristine F-3OCm film, F-3OCm films annealed at 140 °C and 180 °C, and pristine F-3OEt film. The curves in the figure show the trend of the topography change at corresponding positions.

present smooth surface morphologies (Fig. S23 and S24, ESI†). However, after the cyclic processing of the flexible OLEDs, the F-3OEt layers showed obvious black lines in the fluorescence microscopic (FLM) image, associated with the crack formation. The white streaks that appeared in the FLM images of the aged cross-linked F-3OCm films are caused by uneven forces inside and outside the luminescence layer during bending of the flexible device (Fig. 4b), consistent with SEM results. As shown in SEM images displayed in Fig. 4c, a large number of mirco-cracks are clearly observed in the F-3OEt emission layer after 50 cycles of bending the flexible OLEDs up and down, which is the major reason for device fractures. However, it should be noted that a continuous and uniform film morphology with a series of wrinkles appeared in the cross-linked F-3OCm films under same experimental conditions. This excellent deformation stability also reasonably explains the excellent deformation operation of the flexible F-3OCm-based OLEDs.[16]

In the luminance–voltage curves displayed in Fig. 4 and Fig. 25–26 (ESI†), the brightness of OLED devices on flexible substrates was compared with those on glass substrates. Rigid OLEDs based on the pristine F-3OCm film and the F-3OCm films annealed at 140 °C and 180 °C had a maximum luminance of 126.5, 264.9 and 242.8 cd m^{-2}, but the maximum

luminance decreased to 75 cd m^{-2} for the F-3OEt-based OLEDs (Fig. S26 and Table S4, ESI†). Likewise, the maximum brightness for the flexible devices were also similar, with values of 162.0, 296.2 and 242.4 cd m^{-2} for the pristine F-3OCm film and the F-3OCm films annealed at 140 °C and 180 °C, and a value of 17.8 cd m^{-2} for the F-3OEt ones (Fig. 4d and Fig. S27, Table S4, ESI†). It is noteworthy that the current efficiency (C.E.) and external quantum efficiency (EQE) of the flexible devices based on F-3OCm annealed films are maintained at nearly 45%. The C.E. of the device based on the F-3OCm film annealed at 140 °C decreases from 0.537 cd A^{-1} to 0.262 cd A^{-1}, and the EQE decreases from 0.434% to 0.211%; this tendency is also observed for the annealed film obtained at 180 °C (Fig. 4e and Table S4, ESI†). The AFM morphology clearly shows that F-3OEt has more holes but a continuous and uniform surface compared to the F-3OCm emission layer, which seriously reduces the performance of the device (Fig. 4f). OLEDs based on F-3OEt exhibited blue-color emission, similar to the photoluminescence. Surprisingly, OLEDs based on F-3OCm show white-light emission, with the corresponding EL spectrum consisting of two-band emission in the deep-blue and green region, namely, a 400–450 nm band and a new emission at 500–700 nm. To explore the factor responsible for emission at long-wavelength, a small amount of a free-radical trapping agent was added to the luminous layer. As expected, the device displayed blue emission (Fig. S28, ESI†), from which it was inferred that the formation of free radicals under the action of the electric field caused by the styrene double bond resulted in this long-wavelength emission.

Conclusions

In summary, a model small molecule with three cross-linkable styrene units, F-3OCm, was designed and prepared to achieve excellent deformation stability for the fabrication of flexible OLEDs. More interestingly, uniform F-3OCm cross-linked films were achieved *via* thermal treatment at 140 °C and 180 °C and presented efficient and stable deep-blue emission with a high PLQY of ~50%. Compared to the brittleness of the control F-3OEt films, the cross-linked F-3OCm films had excellent intrinsic viscoelastic behaviour with a low Young's modulus and excellent recoverability according to nanoindentation measurements. In addition, the cross-linked F-3OCm films also had excellent stretchable behaviour with tensile rates of >20%. Finally, flexible OLEDs based on the cross-linked F-3OCm films also had excellent deformation and operation stability, due to the continuous and uniform morphology of the emission layer even after being bent up and down 50 times, which was significantly different from the F-3OEt layer, in which a large number of cracks appeared. Therefore, the side-chain cross-linking strategy is an effective tool to improve the stretchability of small-molecule conjugated materials toward flexible optoelectronic devices.

Conflicts of interest

There are no conflicts to declare.

Acknowledgements

This work was financially supported by the National Key R&D Program of China (No. 2020YFA0709900); W. Huang, J. Lin, L. Bai, and Y. Han acknowledge support from the National Natural Science Foundation of China (No. 22075136, 62105262, and 62205141); Y. Han and L. Bai thank the China Postdoctoral Science Foundation (No. 2022M711591); Ning Sun acknowledges support from Postgraduate Research & Practice Innovation Program of Inner Mongolia (B20231018Z); Zhiqiang Zhuo acknowledges support from Postgraduate Research & Practice Innovation Program of Jiangsu Province (KYCX23_1415).

Notes and references

1 Y. Dai, H. Hu, M. Wang, J. Xu and S. Wang, Stretchable transistors and functional circuits for human-integrated electronics, *Nat. Electron.*, 2021, **4**, 17–29.
2 W. Wang, S. Wang, R. Rastak, Y. Ochiai, S. Niu, Y. Jiang, P. K. Arunachala, Y. Zheng, J. Xu, N. Matsuhisa, X. Yan, S. Kwon, M. Miyakawa, Z. Zhang, R. Ning, A. M. Foudeh, Y. Yun, C. Linder, J. B. H. Tok and Z. Bao, Strain-insensitive intrinsically stretchable transistors and circuits, *Nat. Electron.*, 2021, **4**, 143–150.
3 W. Liu, C. Zhang, R. Alessandri, B. T. Diroll, Y. Li, H. Liang, X. Fan, K. Wang, H. Cho, Y. Liu, Y. Dai, Q. Su, N. Li, S. Li, S. Wai, Q. Li, S. Shao, L. Wang, J. Xu, X. Zhang, D. V. Talapin, J. J. Pablo and S. Wang, High-efficiency stretchable light-emitting polymers from thermally activated delayed fluorescence, *Nat. Mater.*, 2023, **22**, 737–745.
4 J. Liang, L. Li, X. Niu, Z. Yu and Q. Pei, Elastomeric polymer light-emitting devices and displays, *Nat. Photonics*, 2013, **7**, 817–824.
5 M. S. White, M. Kaltenbrunner, E. D. Głowacki, K. Gutnichenko, G. Kettlgruber, I. Graz, S. Aazou, C. Ulbricht, D. A. M. Egbe, M. C. Miron, Z. Major, M. C. Scharber, T. Sekitani, T. Someya, S. Bauer and N. S. Sariciftci, Ultrathin, highly flexible and stretchable PLEDs, *Nat. Photonics*, 2013, **7**, 811.
6 G. Pacchioni, Mechanical metamaterials: The strength awakens, *Nat. Rev. Mater.*, 2016, **1**, 16012.
7 J. Xu, S. Wang, G.-J. N. Wang, C. Zhu, S. Luo, L. Jin, X. Gu, S. Chen, V. R. Feig, J. W. F. To, S. Rondeau-gagné, J. Park, B. C. Schroeder, C. Lu, J. Y. Oh, Y. Wang, Y.-H. Kim, H. Yan, R. Sinclair, D. Zhou, G. Xue, B. Murmann, C. Linder, W. Cai, J. B.-H. Tok, J. W. Chung and Z. Bao, Highly stretchable polymer semiconductor films through the nanoconfinement effect, *Science*, 2017, **355**, 59–64.
8 R. Su, S. H. Park, X. Ouyang, S. I. Ahn and M. C. McAlpine, 3D-printed flexible organic light-emitting diode displays, *Sci. Adv.*, 2022, **8**, eabl8798.
9 T. Yokota, P. Zalar, M. Kaltenbrunner, H. Jinno, N. Matsuhisa, H. Kitanosako, Y. Tachibana, W. Yukita, M. Koizumi and T. Someya, Ultraflexible organic photonic skin, *Sci. Adv.*, 2016, **2**, e1501856.
10 L. Bai, Y. Han, J. Lin, L. Xie and W. Huang, Intrinsically stretchable conjugated polymers for flexible optoelectronic devices, *Sci. Bull.*, 2021, **66**, 2162.

11 H. Ling, S. Liu, Z. Zheng and F. Yan, Organic flexible electronics, *Small Methods*, 2018, **2**, 1800070.
12 K. Zhou, K. Dai, C. Liu and C. Shen, Flexible conductive polymer composites for smart wearable strain sensors, *SmartMat*, 2020, **1**, e1010.
13 J. Wan, Y. Xia, J. Fang, Z. Zhang, B. Xu, J. Wang, L. Ai, W. Song, K. N. Hui, X. Fan and Y. Li, Solution-processed transparent conducting electrodes for flexible organic solar cells with 16.61% efficiency, *Nano-Micro Lett.*, 2021, **13**, 44.
14 Y. Tang, R. Li, R. Sun, J. Min, Q. Lin, C. Yang and G. Xie, Flexible all-organic photodetectors via universal water-assisted transfer printing, *Innovation*, 2023, **4**, 100460.
15 X. Zheng, R. Huang, C. Zhong, G. Xie, W. Ning, M. Huang, F. Ni, F. B. Dias and C. Yang, Achieving 21% external quantum efficiency for nondoped solution-processed sky-blue thermally activated delayed fluorescence OLEDs by means of multi-(donor/acceptor) emitter with through-space/-bond charge transfer, *Adv. Sci.*, 2020, **7**, 1902087.
16 H. Hu, X. Guo, Y. Zhang, Z. Chen, L. Wang, Y. Gao, Z. Wang, Y. Zhang, W. Wang, M. Rong, G. Liu, Q. Huang, Y. Zhu and Z. Zheng, Elasto-plastic design of ultrathin interlayer for enhancing strain tolerance of flexible electronics, *ACS Nano*, 2023, **17**, 3921–3930.
17 Y. Fang and J. Xia, Highly stretchable, soft, and clear viscoelastic film with good recoverability for flexible display, *ACS Appl. Mater. Interfaces*, 2022, **14**, 38398–38408.
18 K. D. Harris, A. L. Elias and H. J. Chung, Flexible electronics under strain: a review of mechanical characterization and durability enhancement strategies, *J. Mater. Sci.*, 2016, **51**, 2771–2805.
19 Q. Huang and Z. Zheng, Pathway to developing permeable electronics, *ACS Nano*, 2022, **16**, 15537–15544.
20 N. Matsuhisa, S. Niu, S. J. K. O'Neill, J. Kang, Y. Ochiai, T. Katsumata, H.-C. Wu, M. Ashizawa, G.-J. N. Wang, D. Zhong, X. Wang, X. Gong, R. Ning, H. Gong, I. You, Y. Zheng, Z. Zhang, J. B.-H. Tok, X. Chen and Z. Bao, High-frequency and intrinsically stretchable polymer diodes, *Nature*, 2021, **600**, 246–252.
21 S.-I. Park, J.-H. Ahn, X. Feng, S. Wang, Y. Huang and J. A. Rogers, Theoretical and experimental studies of bending of inorganic electronic materials on plastic substrates, *Adv. Funct. Mater.*, 2008, **18**, 2673–2684.
22 X. An, K. Wang, L. Bai, C. Wei, M. Xu, M. Yu, Y. Han, N. Sun, L. Sun, J. Lin, X. Ding, L. Xie, Q. Zhang, T. Qin and W. Huang, Intrinsic mechanical properties of the polymeric semiconductors, *J. Mater. Chem. C*, 2020, **8**, 11631–11637.
23 J. A. Rogers, T. Someya and Y. Huang, Materials and mechanics for stretchable electronics, *Science*, 2010, **327**, 1603–1607.
24 J. G. Peng and J. Snyder, A figure of merit for flexibility, *Science*, 2019, **366**, 690–691.
25 S. Xu, Z. Yan, K.-I. Jang, W. Huang, H. Fu, J. Kim, Z. Wei, M. Flavin, J. McCracken, R. Wang, A. Badea, Y. Liu, D. Xiao, G. Zhou, J. Lee, H. U. Chung, H. Cheng, W. Ren, A. Banks, X. Li, U. Paik, R. G. Nuzzo, Y. Huang, Y. Zhang and J. A. Rogers, Assembly of micro/nanomaterials into complex, three-dimensional architectures by compressive buckling, *Science*, 2015, **347**, 154–159.
26 D. Yin, J. Feng, R. Ma, Y.-F. Liu, Y.-L. Zhang, X.-L. Zhang, Y.-G. Bi, Q.-D. Chen and H.-B. Sun, Efficient and mechanically robust stretchable organic light-emitting devices by a laser-programmable buckling process, *Nat. Commun.*, 2016, **7**, 11573.
27 T. Li, Z. Y. Huang, Z. C. Xi, S. P. Lacour, S. Wagner and Z. Suo, Delocalizing strain in a thin metal film on a polymer substrate, *Mech. Mater.*, 2005, **37**, 261–273.
28 J. Y. Oh, S. Rondeau-Gagné, Y.-C. Chiu, A. Chortos, F. Lissel, G.-J. N. Wang, B. C. Schroeder, T. Kurosawa, J. Lopez, T. Katsumata, J. Xu, C. Zhu, X. Gu, W.-G. Bae, Y. Kim, J. W. Chung, J. B.-H. Tok and Z. Bao, Intrinsically stretchable and healable semiconducting polymer for organic transistors, *Nature*, 2016, **539**, 411–415.
29 M. W. Jeong, J. H. Ma, J. S. Shin, J. S. Kim, G. Ma, T. U. Nam, X. Gu, S. J. Kang and J. Y. Oh, Intrinsically stretchable three primary light-emitting films enabled by elastomer blend for polymer light-emitting diodes, *Sci. Adv.*, 2023, **9**, eadh1504.
30 C. Wei, L. Bai, X. An, M. Xu, W. Liu, W. Zhang, M. Singh, K. Shen, Y. Han, L. Sun, J. Lin, Q. Zhao, Y. Zhang, Y. Yang, M. Yu, Y. Li, N. Sun, Y. Han, L. Xie, C. Ou, B. Sun, X. Ding, C. Xu, Z. An, R. Chen, H. Ling, W. Li, J. Wang and W. Huang, Atomic-resolved hierarchical structure of elastic π-conjugated molecular crystal for flexible organic photonics, *Chem*, 2022, **8**, 1427.
31 Y. Han, L. Bai, X. An, M. Xu, C. Wei, Z. Lin, M. Yu, J. Lin, L. Sun, N. Sun, C. Wei, L. Xie, X. Ding, Q. Wei, C. Yin, C. Li, W. Su and W. Huang, Intrinsically viscoelastic supramolecular conjugated polymer toward suppressing coffee-ring effect, *CCS Chem.*, 2022, **4**, 3529.
32 B. Liu, L. He, M. Li, N. Yu, W. Chen, S. Wang, L. Sun, M. Ni, L. Bai, W. Pan, P. Sun, J. Lin and W. Huang, Improving the intrinsic stretchability of fully conjugated polymer for deep-blue polymer light-emitting diodes with a narrow band emission: benefits of self-toughness effect, *J. Phys. Chem. Lett.*, 2022, **13**, 7286–7295.
33 J. Ouyang, Application of intrinsically conducting polymers in flexible electronics, *SmartMat*, 2021, **2**, 263–285.
34 A. Shinohara, C. Pan, Z. Guo, L. Zhou, Z. Liu, L. Du, Z. Yan, F. J. Stadler, L. Wang and T. Nakanishi, Viscoelastic conjugated polymer fluids, *Angew. Chem., Int. Ed.*, 2019, **58**, 9581–9585.
35 C. Pan, K. Sugiyasu, Y. Wakayama, A. Sato and M. Takeuchi, Thermoplastic fluorescent conjugated polymers: benefits of preventing π–π stacking, *Angew. Chem., Int. Ed.*, 2013, **52**, 10775–10779.
36 Z. Ding, D. Liu, K. Zhao and Y. Han, Optimizing morphology to trade off charge transport and mechanical properties of stretchable conjugated polymer films, *Macromolecules*, 2021, **54**, 3907–3926.
37 B. Zhao, D. Pei, Y. Jiang, Z. Wang, C. An, Y. Deng, Z. Ma, Y. Han and Y. Geng, Simultaneous enhancement of stretchability, strength, and mobility in ultrahigh-molecular-weight poly(indacenodithiophene-*co*-benzothiadiazole), *Macromolecules*, 2021, **54**, 9896–9905.

38 M. Ni, X. An, L. Bai, K. Wang, J. Cai, S. Wang, L. He, M. Xu, H. Liu, J. Lin, X. Ding, C. Yin and W. Huang, Intrinsically stretchable and stable ultra-deep-blue fluorene-based polymer with a high emission efficiency of ≈90% for polymer light-emitting devices with a CIEy = 0.06, *Adv. Funct. Mater.*, 2022, **32**, 2106564.

39 M.-N. Yu, J.-Y. Lin, Y.-X. Li, H. Soleimaninejad, C.-J. Ou, L.-B. Bai, B. Liu, W. Liu, Q. Wei, Y.-F. Bo, T. A. Smith, D. E. Dunstan, K. P. Ghiggino, L.-H. Xie, C.-X. Xu, D. D. C. Bradley and W. Huang, Emission enhanced and stabilized by stereoisomeric strategy in hierarchical uniform supramolecular framework, *Chem*, 2019, **5**, 2470–2483.

40 F. J. M. Hoeben, P. Jonkheijm, E. W. Meijer and A. P. H. J. Schenning, About supramolecular assemblies of π-conjugated systems, *Chem. Rev.*, 2005, **105**, 1491–1546.

41 C. Ou, N. J. Cheetham, J. Weng, M. Yu, J. Lin, X. Wang, C. Sun, J. Cabanillas-Gonzalez, L. Xie, L. Bai, Y. Han, D. D. C. Bradley and W. Huang, Hierarchical uniform supramolecular conjugated spherulites with suppression of defect emission, *iScience*, 2019, **16**, 399–411.

42 P. Bi, S. Zhang, Z. Chen, Y. Xu, Y. Cui, T. Zhang, J. Ren, J. Qin, L. Hong, X. Hao and J. Hou, Reduced non-radiative charge recombination enables organic photovoltaic cell approaching 19% efficiency, *Joule*, 2021, **5**, 2408–2419.

43 X. H. Jin, M. B. Price, J. R. Finnegan, C. E. Boott, J. M. Richter, A. Rao, S. M. Menke, R. H. Friend, G. R. Whittell and I. Manners, Long-range exciton transport in conjugated polymer nanofibers prepared by seeded growth, *Science*, 2018, **360**, 897–900.

44 A. T. Haedler, K. Kreger, A. Issac, B. Wittmann, M. Kivala, N. Hammer, J. Köhler, H.-W. Schmidt and R. Hildner, Long-range energy transport in single supramolecular nanofibres at room temperature, *Nature*, 2018, **523**, 196–199.

45 J. M. Ha, S. H. Hur, A. Pathak, J.-E. Jeong and H. Y. Woo, Recent advances in organic luminescent materials with narrowband emission, *NPG Asia Mater.*, 2021, **13**, 53.

46 D. Liu, J. De, H. Gao, S. Ma, Q. Ou, S. Li, Z. Qin, H. Dong, Q. Liao, B. Xu, Q. Peng, Z. Shuai, W. Tian, H. Fu, X. Zhang, Y. Zhen and W. Hu, Organic laser molecule with high mobility, high photoluminescence quantum yield, and deep-Blue lasing characteristics, *J. Am. Chem. Soc.*, 2020, **142**, 6332–6339.

47 D. J. Lipomi and Z. Bao, Stretchable and ultraflexible organic electronics, *MRS Bull.*, 2017, **42**, 93–97.

48 N. Sun, H. Gao, L. Sun, J. An, M. Xu, C. Sun, Y. Han, J. Lin, J. Cai, M. Ni, L. He, J. Yang, Z. Wang, L. Bai, X. Zhang, Q. Wei, X. Ding, C. Yin, L. Xie and W. Huang, Enhancement of morphological and emission stability of deep-blue small molecular emitter via a universal side-chain coupling strategy for optoelectronic device, *Chinese Chem. Lett.*, 2022, **33**, 835–841.

49 X. Ding, C. Wei, L. Wang, J. Yang, W. Huang, Y. Chang, C. Ou, J. Lin and W. Huang, Multicomponent flexible organic crystals, *SmartMat*, 2023, e1213.

50 L. Sun, N. Sun, M. Xu, C. Sun, L. Bai, J. Lin, L. Xie, X. Zhang, Q. Wei, Y. Yang and W. Huang, Enhancing the deep-blue emission property of wide bandgap conjugated polymers through a self-cross-linking strategy, *ACS Appl. Polym. Mater.*, 2022, **4**, 2283–2293.

51 L. Bai, Y. Han, C. Sun, X. An, C. Wei, W. Liu, M. Xu, L. Sun, N. Sun, M. Yu, H. Zhang, Q. Wei, C. Xu, J. Lin and W. Huang, Unveiling the effects of interchain hydrogen bonds on solution gelation and mechanical properties of diarylfluorene-based semiconductor polymers, *Research*, 2020, **1**, 3405826.